Naphthalene Included within All-Silica Zeolites: Influence of the Host on the Naphthalene Photophysics

ARTICLE *in* THE JOURNAL OF PHYSICAL CHEMISTRY B · OCTOBER 2001

Impact Factor: 3.3 · DOI: 10.1021/jp012095c

Naphthalene Included within All-Silica Zeolites: Influence of the Host on the Naphthalene Photophysics

F. Márquez,* C. M. Zicovich-Wilson, A. Corma, E. Palomares, and H. García

Instituto de Tecnología Química, Universidad Politécnica de Valencia, CSIC Av. De los Naranjos s/n, 46022, Valencia, Spain

Received: June 1, 2001; In Final Form: August 5, 2001

The photophysical properties of naphthalene within pure silica zeolites were studied by means of diffuse reflectance, steady state and time resolved emission spectroscopy, fluorescence polarization, and FT-Raman spectroscopy. The experimental results indicate that naphthalene is strongly affected by the zeolite host. This distortion is reflected in the bathochromic shift of the 0-0 transition, the shortening of the fluorescence lifetimes, the observation of vibronic couplings, the appearance of room temperature phosphorescence, and the shift to lower vibration energy of the Raman peaks due to the weakening of the naphthalene bonds. The electronic structure of naphthalene within different zeolites has been computed on periodic models by using both the Hartree−Fock and the Kohn−Sham theories and the theoretical 0-0 transitions evaluated from the valence and conduction bands. The theoretical results are in agreement with the experimental observation of a red shift of the 0-0 bands indicating that the naphthalene π electrons are affected by confinement effect.

1. Introduction

Zeolites are organized assemblies with structures of silica in which aluminum has been substituted into a number of the tetrahedral sites.[1,2] The negative charge carried by the aluminosilicate structural unit is balanced by the presence of metal cations that must be in close proximity to the aluminum sites. Simple cations differ substantially in charge, radius, and degree of hydration providing different properties to the zeolite.[3] The framework thus obtained present pores, channels, and cages with different shapes and sizes being able to accommodate guest molecules. Microstructural organization in these systems forms the basis of innovative technologies in petrochemical catalysis and molecular separations, having interesting applications in molecular electronics, integrated optics, and chemical sensing.[4−8]

Many investigations have been devoted to the study of the adsorption of organic molecules in zeolites and the modulation of the photochemical and photophysical processes when they are incorporated into the channels or cavities.[9−21] The properties of the organic guest-zeolite supramolecular assembly are clearly different from the molecular properties of the pure organic due to different factors such as the presence of cations, Si/Al atomic ratio, electrostatic field into the zeolite framework, and channel and pore size. The extent to which one or more of these effects can affect to the organic molecule depends on the type of zeolite used. Thus, the singlet−triplet intersystem crossing is a photophysical process that clearly depends on the cation used as counterion, and its quantum yield can be modulated by changing the cation type.[22−24] The presence of Al in the framework is also related to high electrostatic potentials in the zeolite medium that have been claimed to be responsible for the stabilization of charge separated transient species. The pore and channel sizes are also crucial to understand the different photoprocesses involved under incorporation of guest molecules into the hosts. The influence of the cavity dimensions on the electronic structure of some organic molecules when incorporated within zeolites has been related to the quantum confinement concept,[25] and it has been shown that it is to be responsible for significant changes in the chemical and physical properties of the guest molecules.[21,26−28] These changes can be explained as produced by an "electronic confinement" in which the electron density of the guest is constrained to be mainly localized within the zeolite cavity as a result of the strong short-range repulsion with the electrons of the zeolite walls.[21,26,28]

Studies on the remarkable effects on various photophysical and photochemical processes occurring upon incorporation of aromatic hydrocarbons in zeolites have been reported. Diffuse reflectance, fluorescence, phosphorescence, and IR spectroscopy measurements[22,29−36] have been explored with the aim to understand the processes involved in these systems. Naphthalene has been very often the probe molecule of choice because its photophysics and photochemistry in various media is thoroughly well understood. In this regard, several papers have dealt with the photophysics of naphthalene included within X and Y zeolites, mainly in an attempt to characterize the modulation on some properties by the host.[36]

However, if one wants to study exclusively the influence of the confinement effect avoiding the interference of electrostatic effects due to framework and extraframework charged atoms, it is necessary to prepare samples of pure silica polymorphs of zeolites with different pore dimensions and to use these all-silica zeolites as the host structure. In none of the reports appearing in the literature has this methodology been followed, and discussion of the effect of confinement on the photophysics of naphthalene is flawed by the concurrent contributions of different factors including variations in the framework Si/Al ratio.

In this paper, we report the dramatic variations on the photophysical properties of naphthalene incorporated within pure silica zeolitic structures such as Ferrierite, SSZ24, and ZSM48. We have found that the host−guest interaction is responsible for remarkable effects as the changes in the Raman shift, observation of phosphorescence at low temperature without the

* To whom correspondence should be addressed.

10.1021/jp012095c CCC: $20.00
Published on Web 09/25/2001

presence of heavy cations into the zeolite framework, and the appearance of vibronic activity as derived from fluorescence polarization studies.

2. Experimental Section

Zeolite Synthesis and Characterization. The pure silica Ferrierite was prepared by the fluoride route using Cab-O-Sil, propylamine, pyridine, HF-pyridine, and deionized water in the appropriate amounts.[37] The mixture was stirred until the silica was dissolved and the resulting gels were sealed in containers of 100 mL capacity. Then, containers were placed into a 473 K forced draft oven for 5 days. After that, the contents were filtered and washed with deionized water and subsequently dried at 383 K overnight and calcined in air at 853 K.

Pure silica ZSM48 zeolite was synthesized hydrothermally using hexamethonium hydroxide as templating agent.[38] A total of 0.5 mL of TEOS (tetraethyl orthosilicate) was hydrolyzed with 80 mL of a solution of hexamethonium hydroxide (1 M) for 1 h under stirring. Deionized water was added, and the mixture was transferred into an autoclave and heated at 443 K for 5 days. After this time, the suspension was filtered and washed with deionized water, dried at 383 K overnight, and calcined at 823 K in air for 10 h.

Pure silica SSZ24 was prepared hydrotermally, through the fluoride route, using *N*-methylsparteinium hydroxide (MSPT+) as structure directing agent.[39] MSPT+ was dissolved in water, and subsequently SiO_2 was added in the adequate proportion to obtain a H_2O/SiO_2 ratio in the range of 5−7.5. The mixture was stirred vigorously and transferred to 60 mL Teflon lined stainless steel autoclaves and heated at 448 K under slow rotation for 10 days. After filtration, the solid was washed and dried at 373 K and calcined at 853 K for 3 h.

Phase purity and crystallinity were determined by X-ray diffraction (XRD) using a Philips X'Pert PW3719 instrument (CuKα radiation and graphite monochromator), provided with a variable divergence slit and working in the fixed irradiated area mode. The crystallinity of the zeolites was calculated from the intensity of the 22° 2θ peak in reference to a standard sample.

C combustion analysis was performed in a Fisons analyzer (CHNS-O, EA 1108). Thermogravimetry-differential scanning calorimetry were carried out under air stream using a Netzch thermobalance (STA-409) using kaolin as a standard.

Diffuse reflectance spectra were recorded on a CARY-5 spectrometer by using a Praying Mantis diffuse reflection attachment (Harrick). Samples were packed in a 1-mm sample holder, and the recorded spectrum was converted into Kubelka Munk units by the program supplied with the spectrometer. The background correction was done by recording a spectrum of $BaSO_4$ in the same sample holder. The Kubelka−Munk conversion allows one to transform the intensity value to a magnitude that is linear to concentration according to the following formula:

$$\mathrm{KM} = \left[\frac{\left[1 - \left(\frac{\text{sample}}{\text{background}}\right)\right]^2}{\left[2x\left(\frac{\text{sample}}{\text{background}}\right)\right]}\right]$$

Steady-state fluorescence measurements were performed at different temperatures (ranging from 77 to 293 K) on an Edinburg FS900CDT spectrometer by using a liquid nitrogen cryostat (Oxford Instruments) connected to an ITC-2 controller. Fluorescence lifetime measurements were made using a hydrogen lamp FL900 as the excitation source, a Czerny-Turner monochromator to select the analyzing wavelength and a Hammamatsu photomultiplier tube as the detector.

In the measurements of the fluorescence polarization two polarizers from Polaroid Co. Ltd., with a transmission of 23−25% in the wavelength range of 300−700 nm, and a crossed transmittance less than 0.05% were employed for excitation and emission lights. The degree of polarization, *P*, obtained using the photoselection method[40] was calculated by the following equation:

$$P = \frac{I_{||} - I_{\perp}}{I_{||} + I_{\perp}}$$

where $I_{||}$ and $I_{\perp}$ are the intensities of the emitted light polarized parallel and perpendicular to the exciting light, which is polarized with the electrical vector perpendicular to the plane formed by the excitation and the emission beam. The *P* values were corrected for instrumental factors according to Azumi and McGlynn.[41]

The FT-Raman spectra were recorded on a Bio-Rad spectrometer, model FT-Raman II. The 1.064 nm line of a Nd:YAG laser was used for excitation along with a germanium detector cooled to liquid nitrogen temperature. The Raman spectra were recorded at room temperature in the 180° scattering configuration using high-quality quartz tubes as cells. The laser power at the samples was 70 mW. The Raman spectra were corrected for instrumental response using a white light reference spectrum.

Inclusion of Naphthalene in Zeolites. Zeolites were previously activated by heating at 673 K for 5 h and rapidly cooled in air to room temperature. Zone-refined naphthalene with a purity of 99%, purchased from Aldrich (product number 14,714-1), was recrystallized further from ethanol before use. Naphthalene was dissolved in cyclohexane (Aldrich product number 15,474-1), previously dried by refluxing over calcium hydride. Then, 200 mg of zeolite was added to the solution under continuous stirring at room temperature for 8 h. Next, the zeolite was filtered, washed with cyclohexane, and dried at 423 K. Samples were then sealed within quartz cuvettes under nitrogen atmosphere. The loading of naphthalene incorporated within zeolites, as determined from thermogravimetric and carbon combustion analysis, was ca. 6 mg g^{-1}.

3. Computational Methodology

Four different naphthalene-zeolite adducts have been considered for calculation. Models used are periodic systems where the zeolitic part is simulated by a pure Si framework and the organic part is an array of naphthalene molecules with the same periodicity as the inorganic host. The frameworks considered have the following code label: *BEA, AFI, ZFE, and MEL. In the present calculations, *BEA has the geometry of the c polymorph of the purely silicic Beta zeolite.[42] This particular polymorph has been chosen due to the high symmetry and the relatively low number of atoms per primitive cell. The geometric parameters of AFI and MEL structures are those previously reported for the pure silica SSZ24[43] and ZSM-11 zeolites.[44] Concerning the ZFE framework, geometry is taken from one of the reported polymorphs (UDUD form) of the ZSM48.[45] FER (Ferrierite) was not considered since the unit cell of the framework needs to be expanded to admit the host, resulting in a structure too large to be simulated by ab initio methods.

Naphthalene molecules are located at the channel axis along the plane that matches the largest ellipse diameter of the channel section. The internal geometry parameters of the molecule have

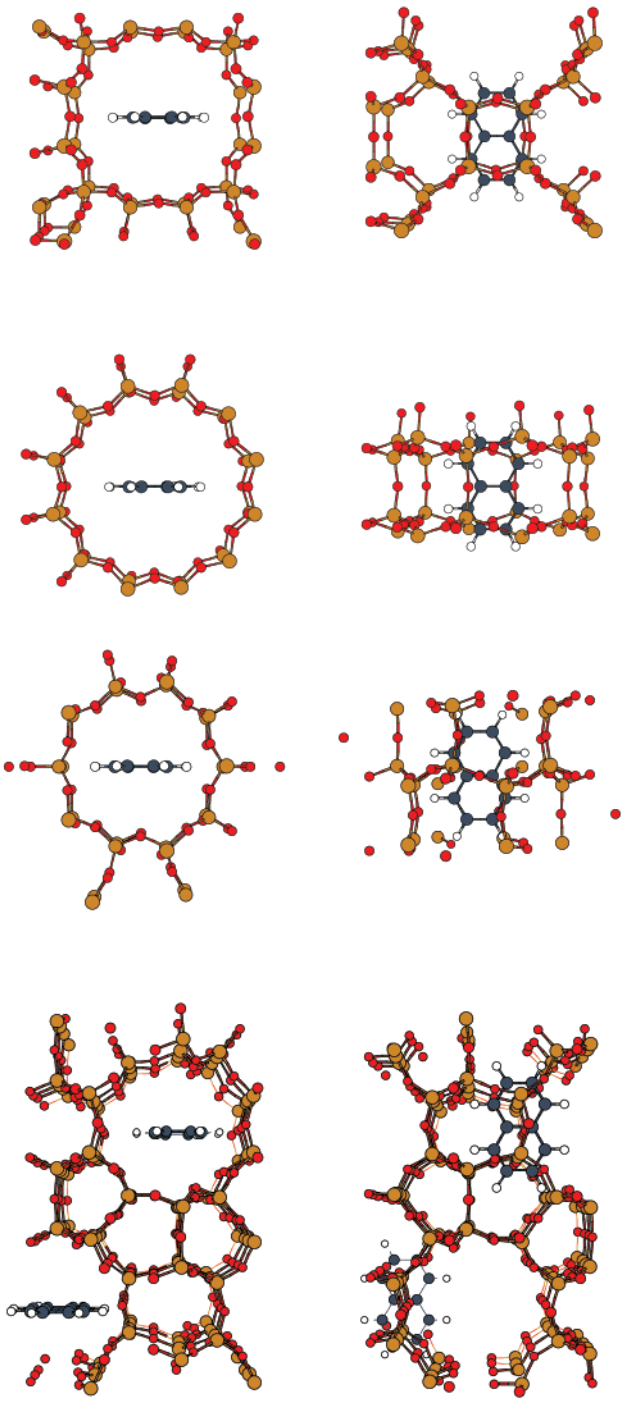

Figure 1. Unit cells of the naphthalene−zeolite models considered for ab initio calculations. Framework types are *BEA, AFI, ZFE, and MEL, from top to bottom. For each model, two views are presented: parallel to the channel axis (left) and perpendicular to the naphthalene plane (right).

been kept fixed at the experimental values.[46] Host−guest models are depicted in Figure 1. The position along the channel axis has been chosen to keep the maximum symmetry of the periodic system. This is because symmetry is exploited in periodic ab initio calculations to increase the computational efficiency.[47] In Table 1 the space group of the clean hosts (h) and the resulting host−guest (h−g) adducts are documented.

Calculations were carried out using the periodic ab initio code CRYSTAL 98.[47] The basis set was a valence double-ζ quality set optimized for periodic calculations. It was the same as reported elsewhere.[26] Hartree−Fock (HF) and Kohn−Sham Hamiltonians have been used to calculate the electronic properties. Concerning the latter, the hybrid Becke 3[48] and the Perdew-Wang 91[49] functionals (B3PW) have been employed for the exchange and correlation terms, respectively. The auxiliary basis set used to expand the exchange-correlation potential has been reported.[50] Tolerances for the truncation of infinite series in the evaluation of the matrix elements are those recommended in the CRYSTAL 98 manual,[47] and the sampling in the Brillouin Zone has been performed using shrinking factor 2.

TABLE 1: Relevant Structural Parameters and Electronic Properties of the Periodic Systems (shown in Figure 1) Considered for ab Initio Calculation

	*BEA	AFI	ZFE	MEL
space group (h)	$P4_2$/mmc	*P6/mcc*	*Imma*	*I4m2*
space group (h−g)	Pmmm	*P2/m*	*Cmcm*	*Imm2*
pore size	9.23	9.80	7.66	7.64
N atoms	114	90	90	162
basis set	1652	1284	1284	2388
$\Delta\epsilon_{HF}$[a]	0.00	−0.07	−0.08	−0.11
$\Delta\epsilon_{B3PW}$[a]	−0.02	−0.06	−0.04	

In Table 1, the basis set dimension and the number of atoms of the periodic models considered are listed. As shown in that table, the systems are quite large, and therefore calculations are to be computationally demanding. In the particular case of MEL, the system size is at the limit of the computational capabilities of a workstation computer for ab initio calculations. This is the reason only a HF calculation could be performed for MEL as the B3PW one exceeded the memory resources of our machine due to the size of the auxiliary basis set. However, in view of the results obtained, this particular data should not add much relevant information. Calculations have been carried out on a Silicon Graphics Origin 200 computer.

4. Results and Discussion

4.1. Experimental Results. The structure of the zeolites used in this work is the following: SSZ24 is a zeolite isostructural with $ALPO_4$-5 (AFI) with cylindrical pores of 7.3 Å diameter defined by 12 T atom rings. ZSM48 is a unidimensional zeolite having 10-member ring channels with a diameter of 5.6 × 5.3 Å. Ferrierite is a member of the pentasil family of zeolites, and its two-dimensional pore structure consists of straight oval 10-ring channels parallel to the *z*-axis that are intersected by cages with 8-ring windows in the *y*-axis. The oval channels (10MR) have pore diameters of 5.4 × 4.2 Å. The diameter of the cages is ca. 7 Å, and the 8MR windows of the cages have diameters of 4.8 × 3.5 Å.

Ground-State Diffuse Reflectance. Diffuse reflectance spectra of pure naphthalene, adsorbed on silica and included within different zeolites, have been previously reported.[51] The spectrum of naphthalene adsorbed on the surface of silica is very similar to that of pure naphthalene, and they are analogous to that recorded in polar solvents (see Figure 2). When naphthalene is included within zeolites, small shifts and differences in intensity appear, being ascribed to effects such as the presence of different environments with different polarity depending on the zeolite type. In the case of pure silica zeolites where the polarity is a constant parameter, we observed small changes that necessarily must be explained as due to factor others than polarity effects.

Luminescence Spectroscopy. Figure 3 shows the room temperature luminescence and excitation spectra of naphthalene, pure and included within zeolites. These spectra are strongly structured showing the vibronic transitions between the S_0 (1^1B_g) and S_1 (1^1B_{1u}) states.[52] The emission spectra closely resemble

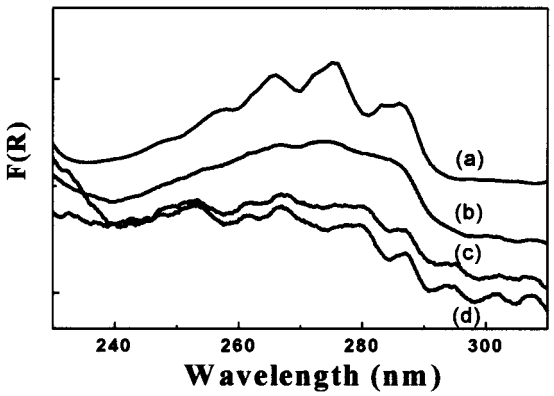

Figure 2. Room temperature diffuse reflectance UV−vis spectra of neat naphthalene and naphthalene included within zeolites. (a) Pure naphthalene, (b) naphthalene in SSZ24 zeolite, (c) naphthalene in ZSM48 zeolite, and (d) naphthalene in Ferrierite. The spectra have been plotted as the Kubelka−Munk function F(R).

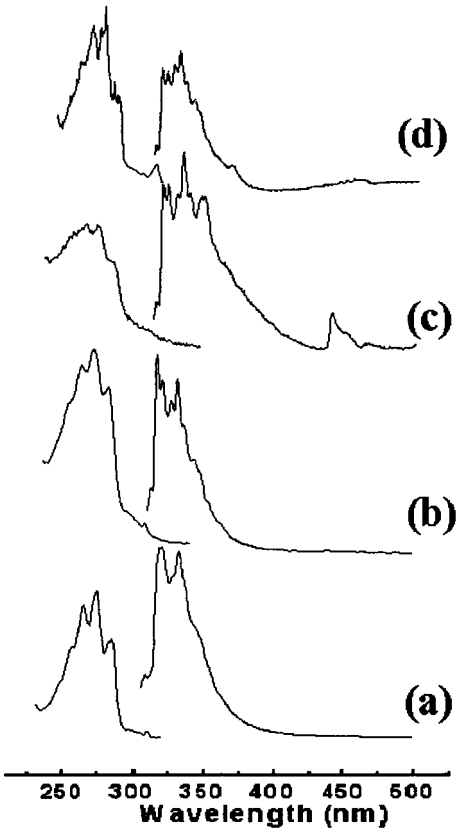

Figure 3. Room temperature excitation (monitored at 320 nm) and emission spectra ($\lambda_{ex} = 276$ nm) of naphthalene crystals (a), naphthalene-SSZ24 (b), naphthalene-ZSM48 (c), and naphthalene-FER (d).

those for crystalline naphthalene showing unique emission behavior except for the case of naphthalene included within ZSM48 zeolite. Surprisingly, an additional emission of naphthalene in ZSM48 is observed (Figure 3), being ascribed to room temperature phosphorescence emission. This effect has only been observed for this zeolite and represents a paradigmatic example of the ability of certain hosts to increase the triplet emission when those are host/guest tight fit.

Interestingly enough, the 0-0 transitions clearly depend on the zeolite. A bathochromic shift going from SSZ24 to Ferrierite can be observed (Table 2). This trend is found to be general, and it may be attributed to the electronic confinement of naphthalene by the zeolite host.

TABLE 2: Photophysical Parameters for Pure Naphthalene Crystals and Naphthalene Included within Zeolites[a]

sample	0-0 (nm)	τ_F (ns)	$\Delta(b_{2u})$ (cm^{-1})
naphthalene	309	66	1382
naphthalene-SSZ24	314	53	1378
naphthalene-ZSM48	315	29	1373
naphthalene-FER	316	17	1372

[a] 0-0 denotes the wavelength of the 0-0 transition, obtained from the excitation and fluorescence spectra, τ_F denotes the fluorescence lifetime, and $\Delta(b_{2u})$ is the wavenumber of the Raman peak corresponding to b_{2u} mode.

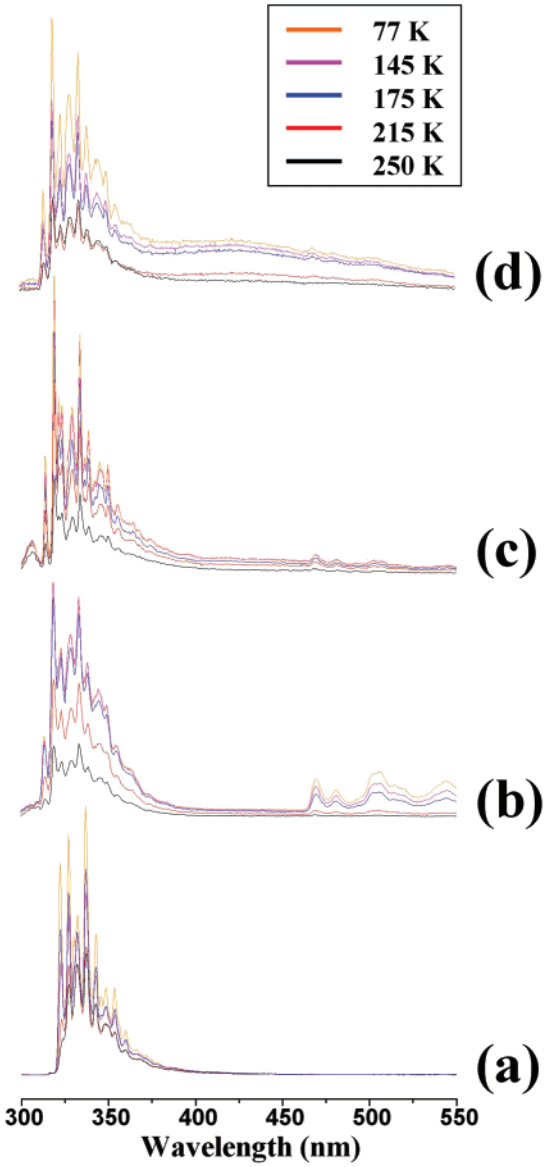

Figure 4. Fluorescence spectra of pure naphthalene and included within zeolites, as a function of temperature. Pure naphthalene (a), naphthalene-SSZ24 (b), naphthalene-ZSM48 (c), and naphthalene-FER (d).

Figure 4 shows the dependence of the emission spectra on the temperature. It should be noted that, at lower temperature, a very structured fluorescence develops. Concomitant with this, the phosphorescence appears. In related precedents, phosphorescence is observed only at very low temperature in deoxygenated media, and it is profoundly affected by the presence of heavy cations. In our present study, naphthalene is included within pure silica zeolites (cation free), and nevertheless it shows phosphorescence from ca. 240 K. Its intensity increases toward

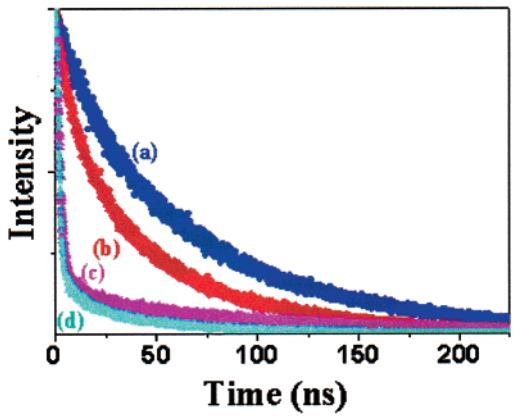

Figure 5. Normalized fluorescence decays of naphthalene monitored at 325 nm after 276 nm excitation of naphthalene (a), naphthalene-SSZ24 (b), naphthalene-ZSM48 (c), naphthalene-FER (d).

lower temperatures. Nevertheless, the phosphorescence intensity is generally very low as compared with the fluorescence emission, except for naphthalene included within SSZ24 zeolite. In this case, the naphthalene phosphorescence to fluorescence intensity ratio is seen to increase linearly as temperature is reduced. As expected in view of the literature data,[53] pure naphthalene does not exhibit phosphorescence in the same range of temperatures indicating that it is its confinement within the zeolite host the factor responsible for this remarkable enhancement of the triplet emission.

Figure 5 shows the room temperature fluorescence lifetimes of naphthalene crystals and naphthalene included within zeolites. The fluorescence lifetime of pure naphthalene can be adjusted to a single-exponential function with a $\tau = 66$ ns (Table 2). The fluorescence lifetime of naphthalene included within zeolites deviates slightly from a single-exponential function but can be adequately fitted by the sum of two exponential decays. These constants are significantly smaller than the 66 ns lifetime of pure naphthalene and clearly depend on the zeolite host. Thus, the fluorescence lifetime decreases from pure naphthalene (66 ns) to naphthalene included in SSZ24 (53 ns) or ZSM48 (29 ns), this effect being more important in Ferrierite (17 ns). This behavior has been previously observed for anthracene[21] and benzene[26] into zeolites, and it has been explained by an "electronic confinement" in which the guest molecule is completely surrounded by the zeolite walls. This effect became specially important when the size of the guest molecules matches the size of the cavities. In general, for conjugated π-systems, the HOMO is more destabilized by the spatial confinement than the LUMO and, as a result, a significant decrease in the HOMO−LUMO gap is expected when the sizes of the cavities and the guest molecules are similar.[21,26−28] Because of this proximity effect, the electronic states involved in the fluorescence mechanism, S_0 and S_1, can become partially degenerated through the vibrational-electronic coupling between both electronic states, enhancing the nonradiative deactivation rate. As a result, the fluorescence lifetime should be dramatically reduced.

Fluorescence Polarization. Figure 6 presents the fluorescence spectrum of pure naphthalene along with the variation of the fluorescence polarization degree of pure naphthalene and naphthalene included in zeolites. In all cases, upon excitation at 276 nm ($\pi\pi^*$) the polarization degree of the 0-0 transition is positive, indicating that the transition moments corresponding to the excitation and fluorescence processes are parallel. In pure naphthalene, the variation of the polarization degree does not

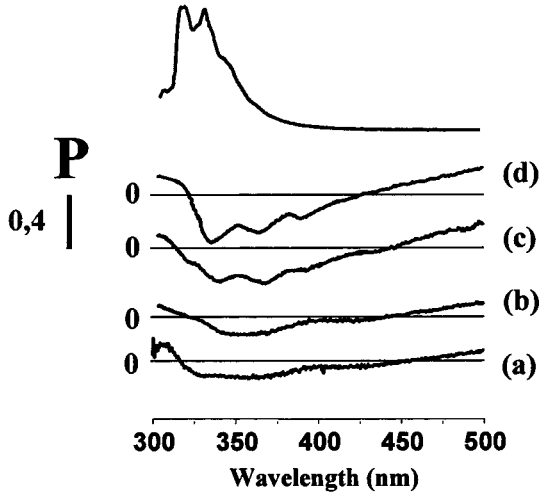

Figure 6. Room temperature fluorescence and polarization spectra of naphthalene (a), naphthalene-SSZ24 (b), naphthalene-ZSM48 (c), and naphthalene-FER (d).

change substantially along the fluorescence band. *P* is positive in the 0-0 band and negative out of this transition.

The polarization degree of naphthalene included within zeolites is also negative out of the 0-0 transition (out-of-plane polarized) with respect to $\lambda = 276$ nm, and this behavior can be connected with the perpendicularity of the excitation and fluorescence transitions moments. As can be seen in Figure 6, the polarization of naphthalene is clearly depending on the zeolite host. Thus, in the case of naphthalene in Ferrierite the change in the polarization degree is not smooth but goes through peaks and valleys, and the *P* value increases with increasing wavelength throughout the emission band. In ZSM48, these oscillating features are also observed, although they are not so pronounced as in Ferrierite. In the case of naphthalene confined within SSZ24, the polarization degree along the fluorescence band is similar to that observed for neat naphthalene.

The changing polarization of naphthalene in Ferrierite and ZSM48, outside the 0-0 transition, and the decrease in the absolute value of the polarization degree throughout the emission band, indicates the presence of vibronic activity that is not observed in pure naphthalene or naphthalene in SSZ24.

This vibronic activity can be correlated with the pore dimensions of the zeolite host. Thus, as previously mentioned, the "electronic confinement effect" induced by the host is responsible for the decrease in the HOMO−LUMO band gap, this effect being more pronounced in Ferrierite and ZSM48. In this way, the presence of vibronic activity in naphthalene confined within zeolites can be justified as due to the "proximity effect" of the electronic states of the organic guest.

FT-Raman Spectroscopy. The near-IR−FT−Raman spectra of naphthalene incorporated within zeolites are presented in Figure 7. The FT-Raman spectrum of neat naphthalene is also compared in Figure 6a showing the most characteristic shifts at 513, 763, 1021, 1381, 1464, 1576, 1628, and 3056 cm^{-1}. The most intense vibration is observed at $\Delta\nu = 1381$ cm^{-1} being attributed to the (b_{2u}) mode. As can be seen in the inset, this vibration clearly experiences a shift of 4 cm^{-1} to low wavenumber when naphthalene is included within SSZ24 zeolite. This shift is remarkably higher in ZSM48 ($\Delta = 9$ cm^{-1}) and Ferrierite ($\Delta = 10$ cm^{-1}) and clearly depends on the size of the zeolite cavity. These variations are significantly larger than the experimental error of the measurements, that is below 1 cm^{-1}. The C−H stretching vibration region between 3000 and 3100 cm^{-1} of naphthalene incorporated within zeolites is similar to

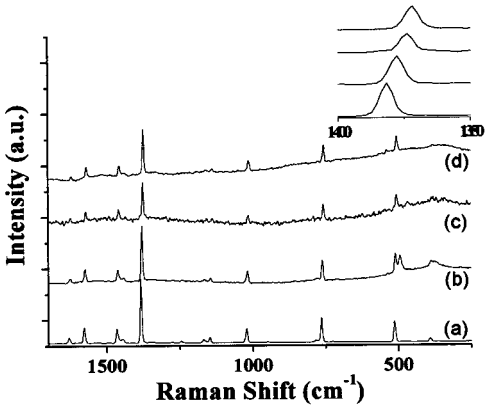

Figure 7. Near-IR−FT−Raman spectra of neat naphthalene (a), naphthalene-SSZ24 (b), naphthalene-ZSM48 (c), and naphthalene-FER (d). The inset shows the shift in the most characteristic band assigned to b_{2u} mode.

that observed in neat naphthalene and does not experience important changes. The influence of the zeolite pore dimensions on the FT-Raman vibrations can be rationalized as due to a confinement effect of naphthalene within the restricted space of the host cavities. This effect should be stronger when the size of the naphthalene molecule approaches the zeolite cage, as occurs in Ferrierite, producing an energy increase of the molecular orbitals, particularly the HOMO. The predicted effect is the decreasing of the HOMO−LUMO band gap and the weakening of the bonds of naphthalene rings, resulting in the shift of the corresponding Raman vibration bands toward lower energy.

4.2. Theoretical Results. The naphthalene band gap included within zeolites has been calculated as the difference between the lowest conduction and the highest valence band maxima in the density of states projected onto the carbon atomic orbitals. Small errors are expected in the estimation of the band gap due to the numerical approximations employed in periodic calculations. These numerical errors are to be more or less significant depending on the particular characteristics of each structure. As one is interested in relative values, such errors can be partially corrected when considering not the absolute band gap but the difference between the actual value and that of a periodic array of naphthalene molecules. The corresponding numerical errors will practically cancel if the array of molecules has the same spatial disposition and is calculated using the same numerical accuracy as in the host−guest system. The calculated band gap differences $\Delta\epsilon$ are listed in Table 1.

Despite the absolute band gap in HF calculations about twice the B3PW ones, the $\Delta\epsilon$ values are of the same order. It is observed in Table 1 that the largest difference between both methods is about 0.04 eV. Except in the *BEA structure, the naphthalene band gap always decreases when the molecule is inside the zeolite cavity. This agrees with previous theoretical studies performed using analytic formulas and a model Hamiltonians approach for the confined system.[25,27,28] There, it has been predicted that spatially confined conjugated π systems feature a smaller band gap than the same system in free state. Additionally, the effect is to be more pronounced when the cavity and molecule dimensions are closer.

The present results show that the decrease in the band gap is about 0.11 eV for the system with the smallest channel size: MEL. However, the expected trend between $\Delta\epsilon$ and pore size is not fully fulfilled. This is due to the discrepancy between the estimated pore size and the effective channel dimension experienced by the electronic structure of the guest molecule, as channels are not uniformly sized along the axis direction. For instance, in *BEA the lowest channel diameter calculated from the distance between opposite bridging O atoms on the cavity surface is smaller than in AFI; however, in the latter $|\Delta\epsilon|$ is unexpectedly larger. *BEA have a tridimensional channel system, and in our model naphthalene is located at the crossing between two 12-ring channels. The effective cavity size is thus larger than in a monodimensional channel system as displayed in AFI, even if the channel diameter is slightly smaller.

An additional source of trouble in the calculated band gap of AFI results from the relative spread of the conduction band related to the naphthalene π system in the density of states. In this particular case, the largest peak in the bottom zone of the conduction band has been considered both in the HF and B3PW, while some quite small peaks appearing at lower energies have been neglected.

5. Summary

In the present work, we have presented experimental and theoretical evidence that the photophysical properties of naphthalene varied upon confinement within pure silica zeolites. The variations observed are summarized below.

(1) The experimental 0-0 transition of naphthalene depends on the zeolite framework and experiences a bathochromic shift from 309 nm (neat naphthalene) to 316 nm (naphthalene in Ferrierite).

(2) In agreement with the experimental measurements, quantum chemistry calculations indicate that the theoretical 0-0 transition should undergo a bathochromic shift whose magnitude is more pronounced when the cavity and molecule dimensions are closer.

(3) The fluorescence lifetimes of naphthalene confined within zeolites are clearly depending on the host and different from neat naphthalene. Thus, whereas the fluorescence lifetime of neat naphthalene is 66 ns, this decay experiences a shortening upon inclusion within SSZ24 (53 ns), ZSM48 (29 ns), and Ferrierite (17 ns). This behavior has been associated with the presence of vibronic interactions that are responsible for the non-radiative deactivation pathway.

(4) Fluorescence polarization of pure naphthalene and naphthalene into SSZ24 are similar and do not show relevant features. In contrast, in the case of naphthalene incorporated within ZSM48 or Ferrierite, with the smallest channel sizes, the changing fluorescence polarization, outside the 0-0 transition, and the decrease in the polarization absolute value indicate the presence of vibronic couplings.

(5) FT-Raman spectroscopy revealed that the C−C vibration bands of naphthalene in zeolites are clearly influenced by the host. This effect is apparently depending on the zeolite cavity and has been rationalized as due to the electronic confinement of naphthalene.

(6) Taken together, the above experimental facts clearly prove that just the mere incorporation phenomenon of a molecule inside the voids of a "chemically inert" microporous solid is sufficient to alter those molecular properties of the guest as a consequence of the changes in the molecular orbitals of the guest. This "electronic confinement effect" is particularly large when a host−guest tight fit occurs.

Acknowledgment. This work was supported by the Spanish CICYT (under contract MAT2000-1392 and MAT2000-1687-102-01).

References and Notes

(1) Corma, A. *Chem. Rev.* **1997**, *97*, 2373.
(2) Meier, W. M.; Olson, D. H.; Baerlocher, C. *Zeolites* **1996**, *17*, 1.

(3) Breck, D. W. *Zeolite Molecular Sieves: Structure, Chemistry and Use*; John Wiley and Sons: New York, 1974.
(4) Stucky, G. D.; MacDougall, J. E. *Science* **1990**, *247*, 669.
(5) Ozin, G. A.; Kuperman, A.; Stein, A. *Angew. Chem., Int. Ed. Engl.* **1989**, *28*, 359.
(6) Eaton, D. *Adv. Synth. React. Solids* **1991**, *1*, 81.
(7) Bein, T.; Enzel, P. *Angew. Chem., Int. Ed. Engl.* **1989**, *28*, 1692.
(8) Bein, T.; Brown, K.; Friye, G. C.; Brinker, C. J. *J. Am. Chem. Soc.* **1989**, *111*, 7640.
(9) Fornes, V.; García, H.; Miranda, M. A.; Mojarrad, F.; Sabater, M. J.; Suliman, N. *Tetrahedron* **1996**, *52*, 7755.
(10) Fornés, V.; García, H.; Jovanovic, S.; Martí, V. *Tetrahedron* **1997**, *53*.
(11) Dutta, P. K.; Tuberville, W. *J. Phys. Chem.* **1992**, *96*.
(12) Doménech, A.; Doménech-Carbó, M. T.; García, H.; Galletero, M. S. *Chem. Commun.* **1999**, 1326.
(13) Doménech, A.; Casades, I.; García, H. *J. Org. Chem.* **1999**, *64*, 3731.
(14) Doménech, A.; Formentín, P.; García, H.; Sabater, M. J. *Eur. J. Inorg. Chem.* **2000**, *6*, 1339.
(15) Cozens, F. L.; García, H.; Scaiano, J. C. *J. Am. Chem. Soc.* **1993**, *115*, 11134.
(16) Cozens, F. L.; García, H.; Scaiano, J. C. *Langmuir* **1994**, *10*, 2246.
(17) Cozens, F. L.; Régimbald, M.; García, H.; Scaiano, J. C. *J. Phys. Chem.* **1996**, *100*, 18173.
(18) Corrent, S.; Hahn, P.; Pohlers, G.; Connolly, T.; Scaiano, J. C.; Fornés, V.; García, H. *J. Phys. Chem. B* **1998**, *102*, 5852.
(19) Corrent, S.; Martínez, L. J.; Scaiano, J. C.; García, H.; Fornés, V. *J. Phys. Chem. B* **1999**, *103*, 8097.
(20) Corma, A.; Fornés, V.; García, H.; Martí, V.; Miranda, M. A. *Chem. Mater.* **1995**, *7*, 2136.
(21) Márquez, F.; García, H.; Palomares, E.; Fernández, L.; Corma, A. *J. Am. Chem. Soc.* **2000**, *122*, 6520.
(22) Ramamurthy, V.; Caspar, J. V.; Eaton, D. F.; Kuo, E. W.; Corbin, D. R. *J. Am. Chem. Soc.* **1992**, *114*, 3882.
(23) Iu, K. K.; Thomas, J. K. *Langmuir* **1990**, *6*, 471.
(24) Iu, K.-K.; Thomas, J. K. *J. Phys. Chem.* **1991**, *95*, 506.
(25) Zicovich-Wilson, C.; Planelles, J. H.; Jaskolski, W. *Int. J. Quantum Chem.* **1994**, *50*, 429.
(26) Zicovich-Wilson, C. M.; Márquez, F.; Palomares, E.; Boronat, M.; Viruela, P.; García, H.; Corma, A. *J. Am. Chem. Soc.* **2001**, submitted.
(27) Zicovich-Wilson, C. M.; Corma, A.; Viruela, P. *J. Phys. Chem.* **1994**, *98*, 10863.
(28) Planelles, J.; Zicovich-Wilson, C. M.; Jaskolski, W.; Corma, A. *Int. J. Quantum Chem.* **1996**, *60*, 971.
(29) García, H.; García, S.; Pérez-Prieto, J.; Scaiano, J. C. *J. Phys. Chem.* **1996**, *100*, 18158.
(30) Gessner, F.; Olea, A.; Lobaugh, J. H.; Johnston, L. J.; Scaiano, J. C. *J. Org. Chem.* **1989**, *54*, 259.
(31) Gessner, F.; Scaiano, J. C. *J. Photochem. Photobiol. A: Chem.* **1992**, *67*, 91.
(32) Ramamurthy, V. Photoprocesses of Organic Molecules Included in Zeolites. In *Photochemisty in Organized and Constrained Media*; Ramamurthy, V., Ed.; VCH: New York, 1991; Chapter 10.
(33) Ramamurthy, V.; Caspar, J. V.; Corbin, D. R. *J. Am. Chem. Soc.* **1991**, *113*, 594.
(34) Ramamurthy, V. *Chimia* **1992**, *46*, 359.
(35) Ramamurthy, V.; Eaton, D. F.; Caspar, J. V. *Acc. Chem. Res.* **1992**, *25*, 299.
(36) Ramamurthy, V. *J. Am. Chem. Soc.* **1994**, *116*, 1345.
(37) Corma, A.; Díaz, U.; Domine, M. E.; Fornés, V. *J. Am. Chem. Soc.* **2000**, *122*, 2804.
(38) Fonseca, A.; Nagy, J. B.; El Hage-Al Assward, J. *Zeolites* **1995**, *15*, 131.
(39) Camblor, M. A.; Villaescusa, L.; Diaz-Cabanas, M. J. *Top. Catal.* **1999**, *9*, 59.
(40) Albrecht, A. C. *Prog. React. Kinet.* **1970**, *5*, 301.
(41) Azumi, T.; McGlynn, S. P. *J. Chem. Phys.* **1966**, *45*, 2413.
(42) Newsam, J. M.; Treacy, M. M. J.; Koetsier, W. T.; Gruyter, C. B. *Proc. R. Soc. London Ser. A* **1988**, *420*, 375.
(43) Benett, J. M.; Cohen, J. P.; Flanigen, E. M.; Pluth, J. J.; Smith, J. V. *Intrazeolite Chemistry*; American Chemical Society: Washington, DC, 1983; Vol. 109.
(44) Fyfe, C. A.; Gies, H.; Kokotailo, G. T.; Paszttor, C.; Strobl, H.; Cox, D. E. *J. Am. Chem. Soc.* **1989**, *111*, 2470.
(45) Schlenker, J. L.; Rohrbaugh, W. J.; Chu, P.; Valyocsik, E. W.; Kokotailo, G. T. *Zeolites* **1989**, *6*, 637.
(46) Rubio, M.; Merchán, M.; Ortí, E.; Roos, B. O. *Chem. Phys.* **1994**, *179*, 395.
(47) Saunders: V. R.; Dovesi, R.; Roetti, C.; Causà, M.; Harrison, N. M.; Orlando, R.; Zicovich-Wilson, C. M. *CRYSTAL98 User's Manual*; Università di Torino: Turin, 1999.
(48) Becke, A. D. *J. Chem. Phys.* **1993**, *98*, 5648.
(49) Perdew, J. P. *Electronic Structure of Solids*; Akademie Verlag: Berlin, 1991.
(50) The CRYSTAL98 Web Page; http://www.ch.unito.it/ifm/teorica/Basis_Sets/mendel.html.
(51) Yamanaka, T.; Takahashi, Y.; Uchida, K. *Chem. Phys. Lett.* **1990**, *172*, 405.
(52) Stevens, B. *Spectrochim. Acta* **1962**, *18*, 439.
(53) Perry, L. M.; Campiglia, A. D.; Winefordner, J. D. *Anal. Chem.* **1989**, *61*, 2328.